Influence of woody elements of a Norway spruce canopy on nadir reflectance simulated by the DART model at very high spatial resolution

Z. Malenovsky, Emmanuel Martin, L. Homolova, Jean-Philippe Gastellu-Etchegorry, R. Zurita-Milla, M. E. Schaepman, R. Pokorny, G.P.W. Clevers Jan, P. Cudlin

Article destiné à être publié à Remote Sensing of Environment 112 (2008) 1-18

Influence of woody elements of a Norway spruce canopy on nadir reflectance simulated by the DART model at very high spatial resolution

Zbyněk Malenovský [a,c,*], Emmanuel Martin [b], Lucie Homolová [c], Jean-Philippe Gastellu-Etchegorry [b], Raúl Zurita-Milla [a], Michael E. Schaepman [a], Radek Pokorný [c], Jan G.P.W. Clevers [a], Pavel Cudlín [c]

[a] *Centre for Geo-Information, Wageningen University, Droevendaalsesteeg 3/PO Box 47, 6700 AA Wageningen, The Netherlands*
[b] *Centre d'Etudes Spatiales de la Biosphère, UPS-CNES-CNRS-IRD, 18 Avenue Edouard Belin, BPI 2801, 31401 Toulouse, Cedex 9, France*
[c] *Institute of Systems Biology and Ecology, Academy of Sciences of the Czech Republic, Na Sádkách 7, 370 05 České Budějovice, Czech Republic*

Received 21 December 2005; received in revised form 21 February 2006; accepted 27 February 2006

Abstract

A detailed sensitivity analysis investigating the effect of woody elements introduced into the Discrete Anisotropic Radiative Transfer (DART) model on the nadir bidirectional reflectance factor (BRF) for a simulated Norway spruce canopy was performed at a very high spatial resolution (modelling resolution 0.2 m, output pixel size 0.4 m). We used such a high resolution to be able to parameterize DART in an appropriate way and subsequently to gain detailed understanding of the influence of woody elements contributing to the radiative transfer within heterogeneous canopies. Three scenarios were studied by modelling the Norway spruce canopy as being composed of i) leaves, ii) leaves, trunks and first order branches, and finally iii) leaves, trunks, first order branches and small woody twigs simulated using mixed cells (i.e. cells approximated as composition of leaves and/or twigs turbid medium, and large woody constituents). The simulation of each scenario was performed for 10 different canopy closures (CC=50–95%, in steps of 5%), 25 leaf area index (LAI=3.0–15.0 m^2 m^{-2}, in steps of 0.5 m^2 m^{-2}), and in four spectral bands (centred at 559, 671, 727, and 783 nm, with a FWHM of 10 nm). The influence of woody elements was evaluated separately for both, sunlit and shaded parts of the simulated forest canopy, respectively. The DART results were verified by quantifying the simulated nadir BRF of each scenario with measured Airborne Imaging Spectroradiometer (AISA) Eagle data (pixel size of 0.4 m). These imaging spectrometer data were acquired over the same Norway spruce stand that was used to parameterise the DART model.

The Norway spruce canopy modelled using the DART model consisted of foliage as well as foliage including robust woody constituents (i.e. trunks and branches). All results showed similar nadir BRF for the simulated wavelengths. The incorporation of small woody parts in DART caused the canopy reflectance to decrease about 4% in the near-infrared (NIR), 2% in the red edge (RE) and less than 1% in the green band. The canopy BRF of the red band increased by about 2%. Subsequently, the sensitivity on accounting for woody elements for two spectral vegetation indices, the normalized difference vegetation index (NDVI) and the angular vegetation index (AVI), was evaluated. Finally, we conclude on the importance of including woody elements in radiative transfer based approaches and discuss the applicability of the vegetation indices as well as the physically based inversion approaches to retrieve the forest canopy LAI at very high spatial resolution.

Keywords: Woody elements; Radiative transfer; DART; Norway spruce canopy; High spatial resolution; LAI; AISA

1. Introduction

Leaf area index (LAI) is a basic structural vegetation parameter mainly controlled by canopy biophysical and morphological processes. LAI is proportionally related to the rate of canopy photosynthesis and consequently to the CO_2 fixation and the net primary production (Ahl et al., 2004; Gower, 2003; Gower et al.,

* Corresponding author. Centre for Geo-Information, Wageningen University, Droevendaalsesteeg 3/PO Box 47, 6700 AA Wageningen, The Netherlands. Tel.: +31 317 474724; fax: +31 317 419000.
E-mail address: zbynek.malenovsky@wur.nl (Z. Malenovský).

0034-4257/$ - see front matter © 2007 Elsevier Inc. All rights reserved.
doi:10.1016/j.rse.2006.02.028

2001; Turner et al., 2003, 2005). A number of studies have successfully demonstrated the effect of physiological vegetation characteristics on climate state (Hoffmann & Jackson, 2000; Zeng & Neelin, 2000; Zhang et al., 2001). In this respect, LAI is acknowledged to be one of the key input parameter for many eco-physiological and climate models describing land surface processes (Arora, 2002; Kucharik et al., 2000). The retrieval of biochemical and biophysical canopy properties, based on radiative transfer methods, represents a universal method that can be applied to both, airborne and satellite imagery (Atzberger, 2004; Fang & Liang, 2005; Koetz et al., 2005; Myneni et al., 2002; Schaepman et al., 2005). Quasi operational LAI products are, therefore, made available very early and achieve currently significant interest from the scientific communities (Knyazikhin et al., 1998; Myneni et al., 1997; Shabanov et al., 2003, 2005; Tian et al., 2002a,b). However, the retrieval models developed for coarse spatial resolution spaceborne sensors are not directly applicable to airborne imaging spectrometers with very high spatial resolution (Gascon et al., 2004).

LAI represents a biophysical structural parameter describing amount of the forest canopy foliage biomass (Monteith & Unsworth, 1990). The structural heterogeneity of a Norway spruce (*Picea abies* (L.) Karst.) canopy foliage is typically increasing with increasing age of the stand due to senescence and the influence of environmental stress agents (Ishii & McDowell, 2002; Remphrey & Davidson, 1992). When the tree crowns become older, irregular structures within the canopy emerge due to the variation in solar irradiation caused by shadowing effects of the neighbouring trees and due to the effect of environmental multiple stress (Taylor, 1998). The foliage distribution (i.e. leaf density and clumping) within a spruce crown is usually a result of such a morphological transformation, starting with specific defoliation processes often followed by systematic regeneration (Gruber, 1994; Nicolini et al., 2001). These physiological processes cause a unique three-dimensional (3D) pattern, resulting in a significant spatially heterogeneous distribution of the leaves and/or shoots (needle sets of one generation) (Ishii et al., 2002). In particular the proportion of woody elements (e.g. trunks, branches, and small twigs) is larger during the defoliation stage resulting in a decrease of LAI. Current research on Norway spruce eco-physiological processes demonstrates possibility to describe mathematically distribution of the canopy foliage and woody structures (Dzierzon et al., 2003; Kuuluvainen & Sprugel, 1996). Consequently, such simplified structural relations can be incorporated into radiative transfer (RT) models, used for estimation of forest canopy bio-chemical and biophysical parameters. Prerequisite for such an approach is that the existing models can be run at a very high spatial resolution, typically with a spatial resolution in the order of a few decimetres, allowing a detailed modelling of all relevant forest canopy structural features.

Destructive ground measurements on 16 Norway spruce trees of our experimental forest stand revealed that brown woody biomass represents about 13% and assimilating green biomass about 87% of canopy surface. The influence of woody elements within a forest canopy have systematically been considered in ground measurements of forest LAI (Chen & Black, 1991; Jonckheere et al., 2004; Kucharik et al., 1998), but has not been largely included in forest RT modelling. Some of the existing RT models consider trunks and branches as solid geometrical objects, for instance the 4-Scale RT model (Chen & Leblanc, 1997; Leblanc et al., 1999), but in general the clumps of small woody particles, irregularly dispersed within the forest canopies, are ignored. Myneni et al. (1997) modelled the trunks and branches as dark objects with a red reflectance equalling to 3.79% and a near-infrared reflectance equalling to 10.02%. However, according to our field measurements of the hemispherical–directional reflectance (HDRF) (Martonchik et al., 2000), the Norway spruce bark may reflect as much as 20–25% between 600–700 nm and even 40–50% between 800–900 nm, resulting in a significantly higher contribution of the woody parts than previously reported. Thus, detailed knowledge of the effect of woody elements on the forest canopy reflectance is essential for designing a refined method retrieving the forest structural parameters (e.g. LAI).

The main objective of this study is to investigate the influence of woody elements (trunks, branches, and tiny twigs) at nadir top of canopy (TOC) reflectance of a Norway spruce stand at very high spatial resolution. The TOC reflectance expressed as bi-directional reflectance factor (BRF) will be simulated using a 3D Discrete Anisotropic Radiative Transfer (DART) model (Gastellu-Etchegorry et al., 1996). In order to validate reliability of the DART images modelled within this study, the forest canopy reflectance of all scenarios is compared against atmospherically corrected hyperspectral images captured by the AISA Eagle airborne sensor. Finally, the sensitivity of two vegetation indices (i.e. Normalized Difference Vegetation Index — NDVI, and Angular Vegetation Index — AVI) and the impact of woody elements therein are discussed as well as their influence on the retrieval of the leaf area index (LAI).

2. Materials and methods

2.1. Test site

The study test site is a montane Norway spruce stand located at the Bily Kriz experimental research site in the Moravian–Silesian Beskydy Mountains (Fig. 1), in the eastern part of the

Fig. 1. Location of the experimental research site Bily Kriz at the Moravian–Silesian Beskydy Mountains (East border between Czech Republic and Slovakia).

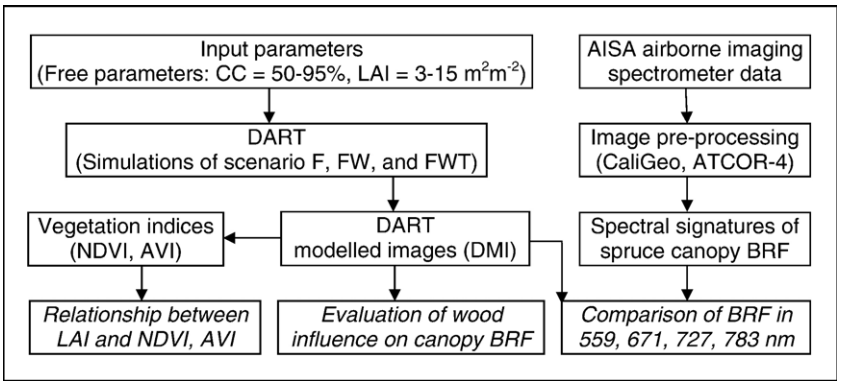

Fig. 2. Flowchart of the methodological approach (scenario F — only foliage elements were simulated; scenario FW — the foliage elements together with trunk and first order branches were simulated; scenario FWT — foliage elements with trunk and first order branches plus small twigs were simulated; CC=canopy closure, LAI=leaf area index, NDVI=normalized difference vegetation index, AVI=angular vegetation index, BRF=bidirectional reflectance factor).

Czech Republic bordering with Slovakia (18.54 °E, 49.50 °N; altitude 936 m above sea level) (Kratochvilová et al., 1989). The geological bedrock of the area is sandstone originating the Mezosoic era. The soil type is a humic podzol combined with loamy sand soil. The humic horizon depth is between 60–80 cm with the gravel fraction of 30–40% and clay fraction of 15–38%. The average annual air temperature is about 5.5 °C, the average annual precipitation amounts to 1000–1400 mm. The snow cover is present in average 160 days per year. The forest stand is made of a regularly spaced plantation of Norway spruce (*Picea abies* (L.) Karst.) trees established with three years old spruce seedlings in 1981. The trees of the monoculture are currently 27 years old (in the year 2005) with an average tree height of 10.6 m, and average diameter at breast height (DBH) of 12.8 cm. Further, the Bily Kriz research site (Pavelka et al., 2003) is also part of the MODIS ASCII Subset project (Oak Ridge National Laboratory Distributed Active Archive Center, 2005b), as well as part of the FLUXNET Global Network (Oak Ridge National Laboratory Distributed Active Archive Center, 2005a) having a flux tower equipped with the typical eddy covariance system measuring the exchanges of carbon dioxide (CO_2), water vapour, and energy between the forest stand and the atmosphere.

2.2. Methodological concept

The overall methodological concept of the study is illustrated in Fig. 2. The DART model was parameterized based on detailed field observations in order to simulate the spectral response of the 27 years old Norway spruce stand. Three scenarios, summarized in Table 1, were applied: i) 'scenario F' — the canopy is only represented by Foliage (leaf elements), ii) 'scenario FW' — the canopy is represented by Foliage and robust Woody parts, i.e. trunks and first order branches (main branches growing directly from the trunk), and iii) 'scenario FWT' — the canopy is represented by Foliage, robust Woody parts, and tiny Twigs, i.e. small branches with a diameter smaller than 1 cm. DART modelled images (DMI) were generated for each scenario and used to evaluate the influence of the woody elements on nadir spruce canopy BRF at the following wavelengths: 559 (green), 671 (red), 727 (red edge), and 783 nm (near-infrared). The measured spruce BRF signatures were extracted from pre-processed high spatial resolution images acquired by AISA Eagle and subsequently a comparison of the DART modelled BRF and AISA measured BRF spectral signatures was carried out. Finally, the sensitivity of two vegetation indices (NDVI, AVI) for LAI was investigated for three different model scenarios. The hypothesis of this study is that the combination of a carefully parameterized DART model supported by extensive ground measurements allows quantifying the influence of the woody parts on TOC BRF of a tree canopy at very high spatial resolution.

2.3. The DART model

The DART model simulates radiative transfer in complex 3D scenes, i.e. urban and natural Earth landscapes possibly with the topography and the atmosphere present. It uses several simulation approaches (e.g. ray tracing, exact kernel and/or discrete ordinate techniques) covering the whole solar reflective

Table 1
Description of the three DART modelled scenarios

Name of scenario	Building units (canopy elements)
F — Foliage	Cells of uniform turbid medium (leaves)
FW — Foliage, Wood	Cells of uniform turbid medium (leaves) Opaque surfaces of geometrical objects (trunks and first order branches[a])
FWT — Foliage, Wood, Twigs	Cells of uniform turbid medium (leaves or tiny twigs[b]) Opaque surfaces of geometrical objects (trunks and first order branches) Mixed cells of turbid media and opaque surfaces[c]

[a] Branches growing directly from the trunk.
[b] Branches smaller than 1 cm in diameter.
[c] Mixed cells can be composed as following combinations: i) diverse mixed turbid media (leaves+tiny twigs), or ii) uniform or mixed turbid media with opaque surfaces (leaves+tiny twigs+first order branches, or leaves+first order branches, or tiny twigs+first order branches).

and emissive part of the electromagnetic spectrum. Since its first release (Gastellu-Etchegorry et al., 1996), its accuracy, range of applications and graphic user interface were significantly improved (Gascon et al., 2001; Gastellu-Etchegorry et al., 2004). The latest DART version has two functioning modes: i) mode *R* (reflective) and ii) mode *T* (thermal). Mode *R* simulates the reflectance of direct sun and/or atmosphere radiation while mode *T* simulates a scene's thermal emission, jointly with a solar emission scenario (e.g. modelling the spectral domain 3–4 μm). In mode *R*, DART is able to make use of a Monte Carlo based simulation approach, capable of modelling very accurately multiple scattering effects. The two major outputs of the DART model are either remotely sensed optical images as well as a 3D radiation budget. The remotely sensed images can be modelled for any urban and natural landscape, atmosphere, wavelength, sun/view direction, altitude and spatial resolution (>0.1 m). DART simulates also directional reflectance factors and brightness temperatures, albedo and also images directly related to the leaf mesophyll, with or without the use of a sensor transfer function.

Any landscape can be simulated using DART as a function of rectangular matrices of parallelepiped cells of any size. These are the building blocks for simulating infinite large scenes. These scenes are usually repetitive in all three spatial dimensions, or partially repetitive for ensuring continuity in the vertical dimension as well as in the infinite slopes. Any scene element is simulated with the help of cells that are composed of turbid media (e.g. a leaf, grass, twigs, air, etc.), plane opaque surfaces of triangles and parallelograms based on parametric reflectance models (e.g. soil, roads, tree trunks and branches of first order, buildings walls and roofs, as well as rivers), or a mixture of all mentioned. The scenes can be very simple (e.g. a layered turbid medium) or rather complex (e.g. urban and natural landscapes) created directly from ancillary digital information such as land cover maps, spectral databases of Earth elements, atmospheric physical and spectral vertical profiles, etc. In addition, the operator can define specific atmospheric quantities, accurately describing the state of the atmosphere (e.g. atmospheric water vapour, aerosol optical depth, urban pollution, etc.). The radiative transfer is tracked by an iterative procedure where one iteration (i) scatters radiation that is intercepted at further iterations ($i+1$). In order to decrease the computational load, the geometric origin of rays may always belong to a predefined grid of points within the sampled cells, or are directly located on the cell facets. Specular and diffuse scattering as well as emissivity of the vegetation and the urban elements are also accounted for. Since DART aims at very high accuracy, also the hot spot phenomenon, multiple scattering, and Earth surface–atmosphere coupling mechanisms are accurately modelled for any sun or viewing direction as well as the aforementioned atmospheric conditions. To maintain modelling consistency, Kirchoffs law ($\varepsilon_d = 1 - \rho_{hd}$) as well as the reciprocity law ($\rho_{hd} = \rho_{dh}$) are verified for simulated turbid media. DART has been successfully tested and validated against field measurements and has also been compared with other models within the RAMI experiment (Pinty et al., 2004). Recently, the DART model was patented (PCT/FR 02/01181) and the industrial version was jointly developed by Magellium Corporation and the Centre National d'Etudes Spatiales (CNES, France).

2.4. Parameterization of the spruce forest stand in the DART model

New forest canopy structural features had to be incorporated into a new DART model in order to allow the parameterization of woody elements. The purpose of this innovation was to increase model reliability and accuracy of the woody forest species simulation at high spatial scales. The Norway spruce architecture in DART comprises a trunk (superimposing parallelepipeds) with branches and a conical crown. The crown is filled with scattering elements distributed in structures of five hierarchical levels: i) trunk, ii) branches, iii) twigs, iv) leaves, and v) empty space. Trunk (i) building within a crown accounts for its heterogeneous structure, i.e. trunk optical and geometrical parameters can vary per defined crown level (l). First order branches (ii) are simulated using four triangles centered along a pre-defined axis at specified zenith and azimuth angles. Tiny woody twigs, i.e. branches smaller than 1 cm in diameter, (iii) are represented by turbid medium cells with specific optical properties, a pre-defined twig density (μ_t) or the twig area index (TAI), and the twig angle distribution (TAD) (Centre d'Etudes Spatiales de la Biosphère, 2005). The leaf volume density (iv) (μ_f) or LAI within a crown vary in vertical as well as horizontal direction following physical distribution functions. Additionally, the mixed cells, containing mixed turbid media (leaves and tiny twigs) and also the geometrical objects (trunk and main branches), can be modeled. The specific LAI of coniferous species is implemented as defined by Chen and Black (1992), proposing the LAI of non-flat leaves to be half the total intercepting leaf area per unit ground surface area. The TAI definition is adapted similarly as

Table 2
Input parameters for the DART scenes used to generate multispectral images for all three study scenarios

Sun position		/Real solar noon/	
Zenith angle	θ_s	[°]	47.80
Azimuth angle (from North clockwise)	ϕ_s	[°]	176.50
Spectral bands		/Full-width-half-maximum — FWHM = 10 nm/	
Green central wavelength	λ_{green}	[nm]	559
Red central wavelength	λ_{red}	[nm]	671
Red-edge central wavelength	λ_{RE}	[nm]	727
Near-infrared central wavelength	λ_{NIR}	[nm]	783
Scene parameters		/Representing a 25 year old Norway spruce forest stand/	
Cell size		[m]	0.20
Horizontal dimensions	x, y	[m]	6.00, 6.00
Number of trees			3–8
Canopy closure (varied parameter)	CC	[%]	50–95/in steps of 5/
Leaf area index (varied parameter)	LAI	[m^2 m^{-2}]	3–15/in steps of 0.5/

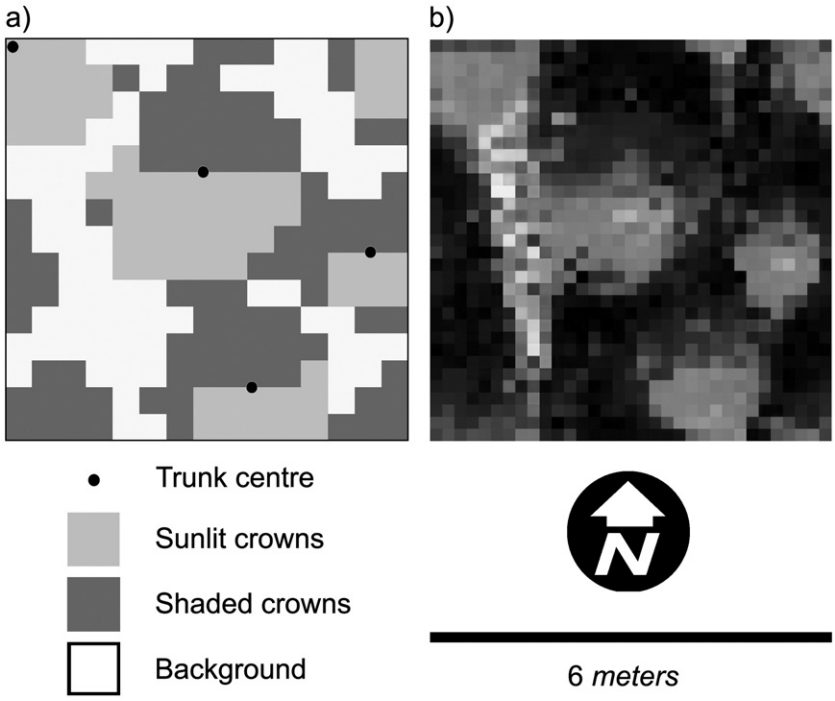

Fig. 3. a) Vertical projection of the DART Norway spruce stand representation with canopy closure of 60% (four representative trees); b) DART output — greyscale image of three spectral band composition (NIR, red, and green band; white = sunlit background, light grey = sunlit crowns, dark grey = shaded crowns, black = deeply shaded crowns and background).

the LAI, being half the total area of woody branches in a diameter smaller than 1 cm/unit ground surface area. Finally, crowns are filled with empty spaces (v) (air gaps) simulating defoliation and clumping of the branches. The defoliation of the canopy is spatially distributed in accordance with recent eco-physiological knowledge of Norway spruce growing strategies (Gruber, 1994). Details about the canopy structural parameters, the design of woody elements, and the radiative transfer through complex forest canopies as implemented in DART are described in the literature published by the Centre d'Etudes Spatiales de la Biosphère (2005) and Malenovský et al. (2003).

Detailed parameterization of the DART model was based on field measurements of the Norway spruce stand at the Bily Kriz research site in September 2004. Ancillary allometric and eco-physiological data of the tree crowns were collected during a field campaign carried out at the same research site in summer 1997 (Pokorný & Marek, 2000). Summary of the DART parameters used for the three scenario simulations is given in Table 2. A repetitive 3D rectangular matrix with a basic cell resolution of 0.2 m represented the forest stand. The total amount of trees and their position within the scene varied according to the simulated canopy closure (CC) category in following way: three trees for the CC of 50% and 55%, four trees for the CC of 60% (Fig. 3a) and 65%, five trees for the CC of 70%, 75% and 80%, six trees for the CC of 85%, seven trees for the CC of 90%, and eight trees for the CC of 95%. The basic allometric parameters (e.g. tree and crown height, bottom crown radius, etc.) reflect the current growing stage of the observed forest stand (Table 3). For each within crown level l, the LAI horizontal distribution is characterized by four parameters: (α(l), β(l), γ(l) and κ(l). The leaf volume density $\mu_f(r)=0$ and $r<\alpha(l)$ with $r>\kappa(l)$, while $\mu_f(r)$ is constant for $r\in[\gamma(l)\ \kappa(l)]$, where r is the horizontal distance from the tree trunk. The

Table 3
Measured parameters of the trees modelled in DART for simulation of all three study scenarios

Tree parameters		/Mean parameters derived for eight individual trees/	
Trunk height below crown		[m]	0.38 (0.13)
Trunk height within crown		[m]	8.08 (0.76)
Trunk diameter below crown		[m]	0.17 (0.02)
Relative trunk diameter within crown		[relative]	0.41 (0.03)
Crown type			Conical
Crown height		[m]	10.08 (0.76)
Crown bottom radius		[m]	1.60 (0.24)
Living crown bottom radius		[m]	1.54 (0.24)
Crown top radius		[m]	0.00
Total tree height		[m]	10.45 (0.88)
Average leaf angle	ALA	[°]	34 (7)
Mean twig area index	TAI	[$m^2\ m^{-2}$]	0.082 (0.017)
Average twig angle	ATA	[°]	35
Number of crown levels			10
Relative height of one tree level		[relative]	0.09
α parameter of horizontal leaf distr.	α	[relative]	0.00
β parameter of horizontal leaf distr.	β	[relative]	0.34
γ parameter of horizontal leaf distr.	γ	[relative]	0.63
κ parameter of horizontal leaf distr.	κ	[relative]	1.00
a parameter of horizontal hole distr.	a	[relative]	0.15
b parameter of horizontal hole distr.	b	[relative]	1.00
Percentage of full leaf cells within crown		[%]	48.00

Values in parenthesis stand for standard deviation (SD).

horizontal distribution of holes is defined by two parameters: a (l) and b(l), where total defoliation (i.e. 100% empty cells) is defined for distances of $r<p$ and $r>b$, and the specific proportion of leaf/empty cells is defined for $r\in[a(l)\ b(l)]$. The horizontal distribution of needles was derived from the analysis of 24 sample branches cut off from the bottom, middle and top part of the eight sample tree crowns. This analysis also provided information on branch foliage clumping, i.e. spatial distribution of empty spaces (air gaps) among shoots (so called random mosaic defoliation), and also location of the 100% defoliated zones (so called inner crown defoliation) (Cudlín et al., 2001). The vertical distribution of green biomass (apparent leaf volume density μ_f) is parameterized by crown foliage destructive measurements carried out on 16 trees of the same age during summer 1997. The leaf angle distribution (LAD) was defined as ellipsoidal (Campbell, 1990), computed from the crown level specific average leaf angle (ALA) of 25° for two upper crown levels, 30° for two middle upper crown levels, 35° for two middle lower crown levels, and 40° for last four bottom crown levels. ALA values were derived through a combination of the needle angular distribution within the shoot and shoot angular distribution within the crown. Trunks were defined as the superimposition of parallelepipeds with different height and side size for each vertical crown level l. The thickness of the trunk within crown is computed based on the trunk diameter out of crown (e.g. DBH) multiplied by a relative trunk diameter specific for each vertical crown level l (Table 3). Two whorls of first order branches, defined for each distinct vertical crown level, consisted of 4–6 branches. Small woody twigs, treated as uniform turbid cells of fine wood or cells mixed with foliage and first order branch triangles, were specified in a radius of 0.2 m around the first order branches. The ellipsoidal twig angle distribution (TAD) is equal to the average shoot angle, which was measured to be on average 35° for the whole canopy.

The optical properties, i.e. integrated hemispherical–directional reflectance and transmittance, of the canopy elements (leaves and bark of the woody parts) and background elements (litter and bare soil) were obtained from laboratory measurements. These were performed under artificial illumination in an integrating sphere LI-1800-12 (Li-Cor, Inc., Lincoln, NE, USA) (Li-Cor, 1983) coupled with a laboratory/field spectroradiometer ASD FieldSpec Pro FR (Analytical Spectral Devices, ASD Inc., USA) in September 2004. The needle samples of last three generations from the sunlit crown part (3rd branch whorl from the top) and the shaded crown part (7th branch whorl from the top, inside a crown) were collected from ten selected trees of the experimental forest stand. The needle optical properties were measured according to the improved methodology proposed by Daughtry et al. (1989) and revised later by Middleton et al. (1997) and Mesarch et al. (1999). The laboratory spectral measurements range between 350 and 2500 nm in steps of 1 nm. Determination of the needle optical properties representative for each distinct crown level is based on a percentage distribution of the needle age classes

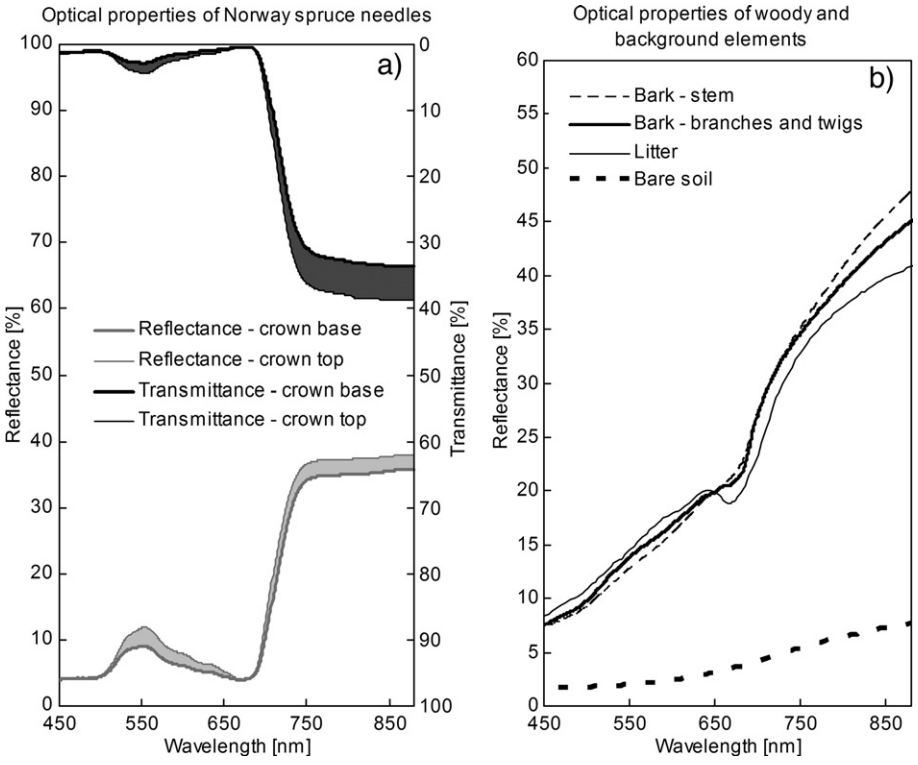

Fig. 4. Measured optical properties (hemispherical–directional reflectance and transmittance) of the surfaces used to parameterize the DART simulations: a) ranges of the Norway spruce needle optical properties defined from base to top of the crown, b) optical properties of woody elements (bark of stem, branches and twigs) and background (litter and bare soil).

and an appropriate ratio of the sunlit and shaded needles within seven vertical crown zones (Fig. 4a). The reflectance properties of the trunks within the scene are computed as the average of five bark HDRF measurements. It was unfeasible to measure optical properties of the tiny twig bark due to the too small cylindrical shape of fine twigs. Therefore, the bark optical properties of first order branches are assumed to be similar to the twig bark properties (c.f. Fig. 4b). Due to the absence of the vegetation understory the HDRF of the background is specified by an equal proportion of litter (senescent needles) and bare soil reflectance given in Fig. 4b. Because the used integrating sphere LI-1800-12 was not designed to measure specular and diffuse reflectance separately, the optical properties of all the modelled elements represent an integration of both values, and subsequently had to be assumed and defined in DART as being of lambertian nature.

2.5. DART modelled images

In total 250 simulations per scenario were performed for four spectral bands, each using DART 2005. These simulations are the result of all possible combinations of CC between 50 and 95% (in steps of 5%) and LAI from 3.0 to 15.0 m^2 m^{-2} (in steps of 0.5 m^2 m^{-2}). The ranges of the CC and LAI were set according to the minimal and maximal values measured within the spruce stand at Bily Kriz research site. The diffuse hemispherical irradiation was not simulated within the scenes, resulting the DART to simulate spectral images representing top of canopy bidirectional reflectance factor (BRF). BRF is defined as being a function of the solar illumination direction (θ_s, ϕ_s), surface reflection direction (θ_r, ϕ_r), and spectral wavelength λ (Schaepman-Strub et al., 2005). DART modelled images at 0.2 m spatial resolution (e.g. Fig. 3b) were aggregated by means of a bilinear resampling to a pixel size of 0.4 m in order to match the AISA Eagle image resolution. The very high spatial resolution allowed the selection of pure spruce canopy pixels, avoiding potential disturbing effects of sunlit as well as of shaded background of litter and soil. Therefore, sunlit and shaded pixels of the tree crowns were delineated from the DART simulated nadir BRF images and an average reflectance of these pixels was separately extracted. The sunlit crown parts are in this study defined as the spruce canopy surface being insolated directly by the sun, i.e. the crown turbid cells interacting with direct solar irradiation. The sunlit crown pixels were easily distinguishable by means of high BRF intensity (mainly in the NIR). The area of the shaded crown is defined by the crown turbid cells not interacting with direct solar irradiation, i.e. the spruce canopy surfaces at the dark side of crowns or shaded by the tree crowns in their neighbourhood. Since spatial resolution of the DART leaf turbid cell was set to 0.2×0.2 m, an aggregated image (pixel size of 0.4 m) composed of sunlit pixels may contain a minor ineffective fraction of shaded leaf turbid cells. Finally, we have defined the overall canopy reflectance as mean BRF of all sunlit and shaded spruce crown pixels. The effect of the woody elements on the BRF, as well as on the vegetation indices, was evaluated from the DMI of the three scenarios separately for the sunlit and shaded crown parts, and also for the overall spruce canopy.

2.6. AISA Eagle airborne image data

Several flight lines above the montane Norway spruce forest stands of the Bily Kriz experimental research site were acquired using the Airborne Imaging Spectroradiometer (AISA) Eagle pushbroom VNIR airborne scanner (Spectral Imaging, SPECIM Ltd., Finland) starting 11:50 a.m. (GMT) on September 18th 2004 (Fig. 5). 64 spectral bands with a Full-Width-Half-Maximum (FWHM) of about 10 nm and a spatial resolution of 0.4 m were acquired in the spectral range from 398.39–

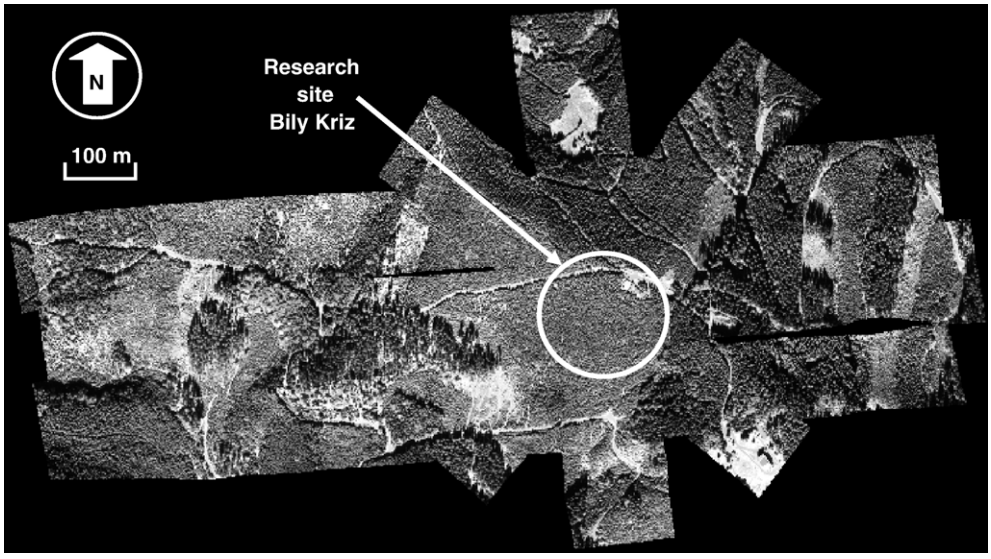

Fig. 5. Six ortho-rectified flight lines acquired by the airborne AISA Eagle imaging spectroradiometer in a multi-directional pattern with the pixel size of 0.4 m over the permanent experimental research site Bily Kriz (Beskydy Mts., Czech Republic; 18.54 °E, 49.50 °N, altitude 936 m above sea level; greyscale image of NIR, red, and green band composition).

983.06 nm. The AISA images were acquired under the clear sky conditions (no clouds, visibility >30 km) implying a low portion of diffusely scattered light compared to the direct solar illumination. Radiometric correction to radiance values was performed using the CaliGeo software (Spectral Imaging, SPECIM Ltd., Finland), parameterized by the sensor specific calibration coefficients. The atmospheric correction was performed in two steps. Fist we used the empirical line method (Smith & Milton, 1999) to convert at-sensor radiances to surface reflectance (HDRF). The concept of the HDRF is similar to the BRF definition except that illumination is coming from the entire upper hemisphere (Martonchik et al., 2000). For the empirical line correction we used a set of five lambertian calibration panels (each 2.5×2.5 m large in size, placed on the flat ground) with a flat response curve ranging from 5% to 70% within the visible and NIR wavelengths (Clevers, 1988). Their nadir reflectance (HDRF) was measured in a field with the ASD FieldSpec Pro spectroradiometer during the AISA image acquisition. The quality control of the data revealed a brightness gradient within the airborne images in across-track direction, mainly due to the large field of view (FOV=29.9°). Therefore, a nadir normalization method was applied to convert HDRF to BRF using ATCOR-4 (Richter & Schlapfer, 2002). The resultant radiometric quality of the data was verified with the reflectance of three independent calibration targets (i.e. clay, gravel, and homogeneous grass cover). Three spots of each target, clearly visible on the AISA images, were measured during the flight with the FieldSpec Pro spectroradiometer (50 scans per one measurement) and averaged. The size of the measured calibration sites extends far beyond the AISA pixel size, allowing for selection of pure reflectance spectra uncontaminated by the adjacency effects. Finally, the AISA BRF images were geo-orthorectified using the Universal Transverse Mercator (UTM) geographic projection (zone 34 North) in combination with a digital elevation model having 2 m vertical resolution and 0.4 m horizontal resolution. The geo-referencing was accomplished also using ancillary data about the aircraft position recorded during the image acquisition by the Aerocontrol IIB system (Ingenieur–Gesellschaft für Interfaces, IGI GmbH, Germany) composed of an Inertial Measurement Unit (IMU) combined with a Global Positioning System (GPS). The achieved positional accuracy is about 1.2 m (3 pixels) in the horizontal directions.

2.7. Comparison of DART and AISA Eagle BRF's

The results of the DART simulations were validated with BRF of the AISA image. A regular network of 14×3 points (at distances of 5 m) was established within the experimental forest stand (Fig. 6). Precise geographic position of the points in UTM geographic projection (zone 34 North) was measured with a Differential Global Positioning System (DGPS) using TRIMBLE 4700 and 4800 receivers (Trimble Navigation Limited, USA) in combination with an Impulse 200 Laser Rangefinder and a MapStar electronic compass (Laser Technology Inc., USA), controlled by a Field Map data collecting system (Institute of Forest Ecosystem Research, IFER Ltd., Czech Republic). A set of hemispherical photographs was taken at each sampling point with a Nikon Coolpix 8700 digital camera (Nikon Corporation, Japan) equipped with a fish-eye lens (FOV=180°). Hemispherical images were processed by the CAN EYE software (Weiss, 2004) to extract LAI of the spruce canopy for 12 matrices of 3×3 points (10×10 m). The vector file containing the 12 matrices was superimposed on the geo-rectified AISA Eagle image as shown in Fig. 6 to locate the observation points. A maximum likelihood (MLH) supervised classification (Strahler, 1980) of the AISA image was used to distinguish the categories of sunlit and shaded spruce canopy and sunlit and shaded ground within each matrix. The MLH classification of the matrices was applied to create masks of sunlit and shaded crown parts. Subsequently, the percentage of sunlit and shaded canopy pixels in each matrix was used to estimate the canopy closure (CC). CC was calculated as the ratio of the number of pixels classified as sunlit or shaded (i.e. pixels of overall spruce canopy) against the total number of pixel within a matrix. The combination of measured LAI and image derived CC of each matrix was used as the primary key to search through the DMI and retrieve corresponding overall canopy BRF of each simulated scenario. Finally, the AISA image derived spruce canopy BRF of four selected bands was compared with the canopy BRF values of corresponding DART modelled images.

2.8. NDVI and AVI vegetation indices

The vegetation indices are specifically designed to detect changes in physical or chemical properties of the observed

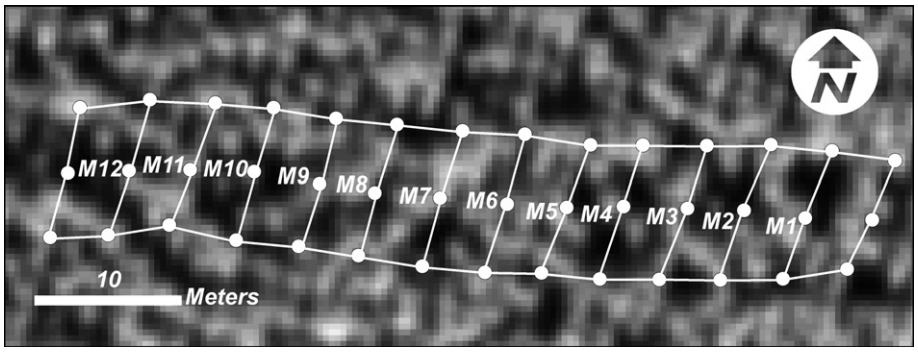

Fig. 6. BRF validation matrices, used also for the measurement of the forest stand leaf area index (LAI), plotted over the grey-scale AISA Eagle band (738 nm). M1–M12 stands for centres of 12 validation matrices of 3×3 points (10×10 m; one circle represents one sampling point).

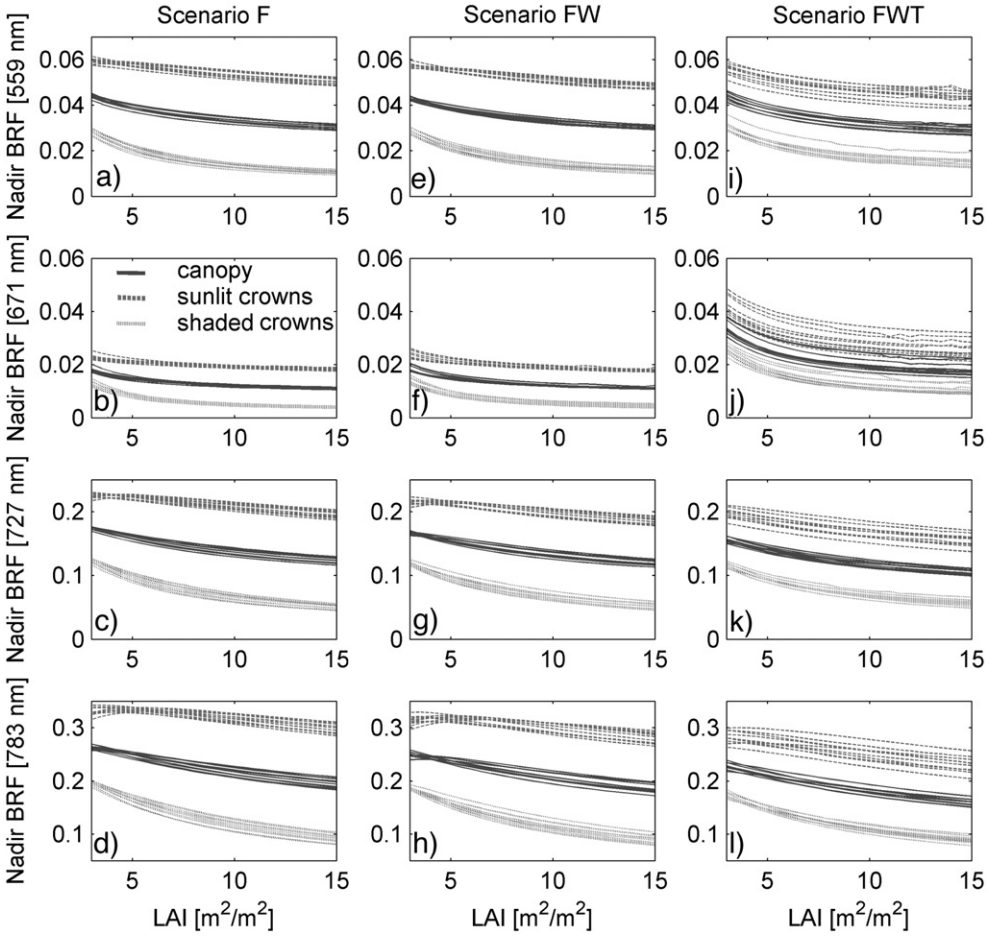

Fig. 7. Relation of DART nadir bidirectional reflectance factor (BRF) and LAI simulated at 559, 671, 727, and 783 nm within the Norway spruce canopy composed of i) only foliage (scenario F: a–d), ii) leaves and major woody parts (scenario FW: e–h), and iii) leaves, trunks, branches of first order, and twigs smaller than 1 cm in diameter (scenario FWT: i–l). Light grey dashed lines represent BRF of sunlit crown pixels of 10 canopy closures (CC=50–95% with step of 5%), black dotted lines represent BRF of shaded crown pixels of 10 canopy closures, and dark grey full lines represents BRF of 10 canopy closures of the whole spruce crowns.

objects from their reflected radiation (Bannari et al., 1995). Physically based radiative transfer models offer the flexibility to design, test and vary spectral vegetation indices computed at different spatial, spectral and directional resolution (Broge & Leblanc, 2001; Haboudane et al., 2002). We use two vegetation indices to demonstrate independently the sensitivity of them to the presence of woody elements simulated in three DART scenarios at the very high spatial resolution. The Normalized Difference Vegetation Index (NDVI) was designed to distinguish vegetation from other objects (bare soil, snow, water, clouds) (Rouse et al., 1973). It is a traditional index based on reflectance differences at visible and NIR wavelengths:

$$\mathrm{NDVI} = \frac{(\rho_{\mathrm{NIR}} - \rho_{\mathrm{red}})}{(\rho_{\mathrm{NIR}} + \rho_{\mathrm{red}})}, \tag{1}$$

where ρ_{NIR} is the near-infrared reflectance and ρ_{red} is the red reflectance. Early research indicated a close statistical relationship between the NDVI and the LAI (Jordan, 1969; Tucker, 1979), but several more recent studies reported low correlation of these two variables in dense canopies (Fassnacht et al., 1997; Lee et al., 2004; Turner et al., 1999), as well as for spectral data at high spatial resolution (Gascon et al., 2004). The second index, called the Angular Vegetation Index (AVI), is based on a geometric concept of the angle defined between reflectances at green, red, and near-infrared wavelength (Plummer et al., 1994):

$$\mathrm{AVI} = \frac{2\left(\pi - \left(\left(\frac{\pi}{2} - \tan^{-1}\frac{(\lambda_{\mathrm{red}}(\rho_{\mathrm{NIR}} - \rho_{\mathrm{red}}))}{(\lambda_{\mathrm{NIR}} - \lambda_{\mathrm{red}})}\right) + \left(\frac{\pi}{2} - \tan^{-1}\frac{(\lambda_{\mathrm{red}}(\rho_{\mathrm{green}} - \rho_{\mathrm{red}}))}{(\lambda_{\mathrm{red}} - \lambda_{\mathrm{green}})}\right)\right)\right)}{\pi}, \tag{2}$$

where ρ_{NIR} is the near-infrared reflectance at the wavelength λ_{NIR}, ρ_{red} is the red reflectance at the wavelength λ_{red}, and ρ_{green} is the green reflectance at the wavelength λ_{green}. The spectral bands used for the AVI computation in this study were selected from the available simulated wavelengths as following: ρ_{green}=559 nm, ρ_{red}=671 nm, and ρ_{NIR}=783 nm. This angular index was designed in order to eliminate the influence of soil background and atmospheric aerosols (North, 2002). However, the sensitivity of the index for presence of woody elements in a canopy has not been previously investigated.

3. Results

3.1. Effect of non-photosynthetic woody elements on nadir spruce canopy BRF

In general, the DART modelled images of all three scenarios show a negative relationship between LAI and BRF of all four bands (Fig. 7). This general trend of descending reflectance can be explained by a larger photon absorbance ability of the forest canopy with higher foliage density μ_f composed in more leaf layers. In other words, as leaf foliage density increases, the crown absorption increases and simultaneously the crown transmittance decreases. This limits the amount of photons available for scattering at crown elements of lower canopy levels and the background (soil). Final canopy BRF is composed of radiation reflected directly from the insolate crown elements (radiation of specular and diffuse nature) and radiation scattered back from the lower crown parts and background (radiation of only diffuse nature). The results in Fig. 7 suggest that intensity increase of the first mentioned canopy BRF components are smaller with growing leaf density (LAI) than the decrease of the second diffuse component.

The reflectance of sunlit crown parts and specified CC for scenario F ranged between 5 and 6% in the green, around 2% in the red, 19–23% in the RE, and 29–35% in the NIR band. As expected the reflectance of shaded pixels was lower, gaining about 1–3% in the green, 0–1% in the red, 5–12% in the RE, and 5–20% in the NIR. The overall canopy reflectance, computed as being the mean of the sunlit and shaded crown pixels, was approximately 3–5% in the green, 1–2% in the red, 11–18% in the RE, and 20–27% in the NIR band, respectively (c.f. Fig. 7abcd). The spectral variability between the CC steps at all LAI classes was quite low. In scenario FW, after the introduction of the trunks and first order branches, the relationship between LAI and BRF did not change significantly (Fig. 7efgh). Only nadir reflectances of sunlit crowns at 783 nm decreased about 2–3%. All the other cases showed only negligible change, less than 1%. Finally, strong changes were observed for the FWT scenario (Fig. 7ijkl). The introduction of accurate modelling of small twigs by means of the mixed cells increased the canopy spectral heterogeneity, which resulted in higher variability and irregularity within the CC spectral responses per LAI (mainly sunlit crown parts). The BRF of the sunlit pixels in the green slightly decreased down to 4–6%,

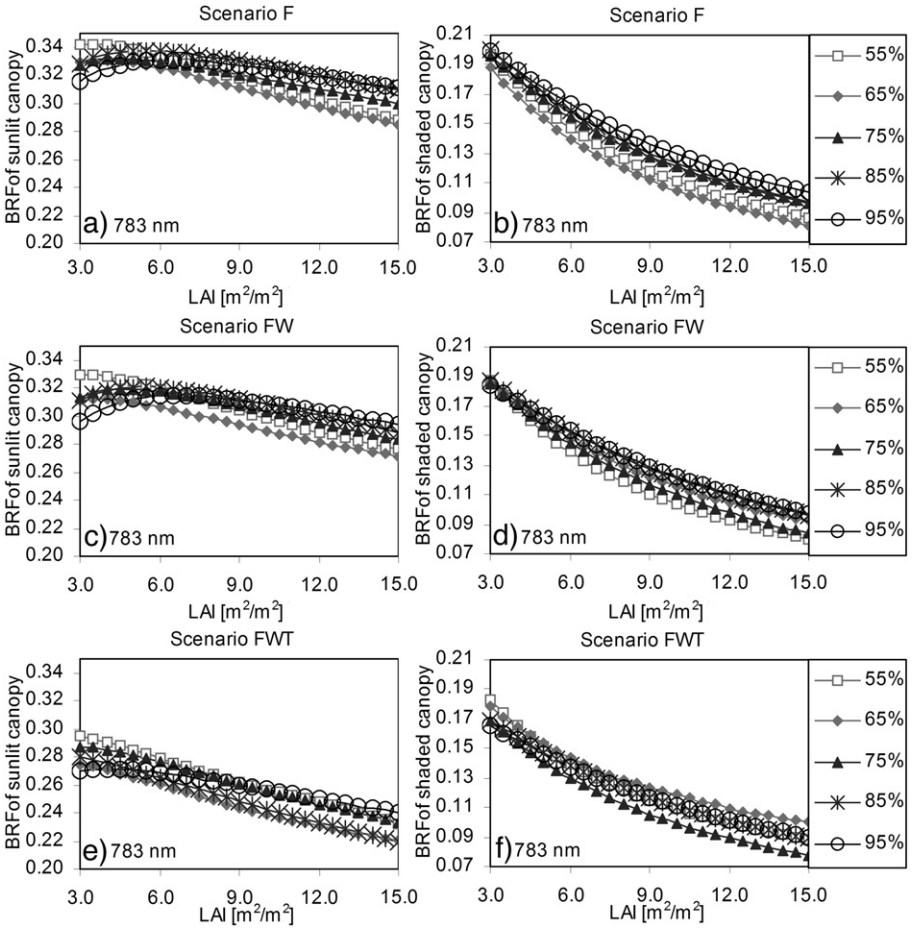

Fig. 8. Detailed relationship of the canopy leaf area index (LAI) and the bidirectional reflectance factor (BRF) of the sunlit and shaded crown parts at 783 nm simulated by the DART model for five different canopy closures (CC = 55, 65, 75, 85, and 95%) for each of the three scenarios: i) scenario F — only foliage (a, b), ii) scenario FW — leaves and major woody parts (c, d), and iii) scenario FWT — leaves, trunks, main branches, and small twigs (e, f).

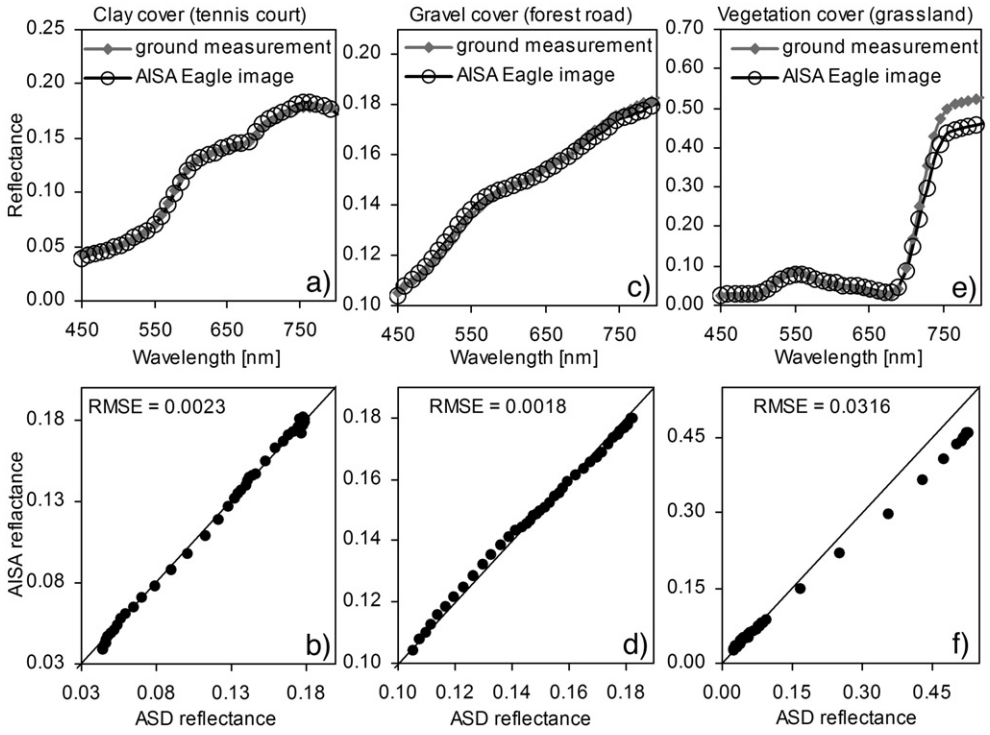

Fig. 9. Validation of the AISA Eagle image radiometric and atmospheric corrections by comparison with ground measured ASD reflectance of three natural surfaces (50 scans per spot, three spots per surface): clay cover (tennis court — a, b), gravel cover (forest road — c, d), and homogeneous vegetation cover (grassland — e, f). The upper graphs show the reflectance signatures of both instruments, the lower graphs represent the relationship between the ground measured reflectances (HDRF) and the image-derived reflectances in the spectral range of 450–800 nm (RMSE=root mean square error).

in the red increased up to 3–5%, and in the RE and NIR band decreased down to 15–20% and 20–30%, respectively. The BRF of the shaded pixels remained more stable, meaning that there was minor change of about 1% for the CC reflectances at the RE and about 3% at the NIR wavelengths. The BRF of the green band increased above 3%, and BRF of the red band increased up to 1–3%. Finally, the overall canopy reflectance for the FWT scenario remained almost unchanged for the 559 nm wavelength, decreased slightly for longer wavelengths at 727 and 783 nm, and increased at 671 nm wavelength by means of about 2–3%.

Closer investigation of the nadir reflectances simulated at 783 nm (Fig. 8) revealed that the BRF values for higher sunlit CC signatures (CC>55%) of scenario F and FW display a non-monotonic, skewed Gaussian-like, behaviour. It is obvious that more than one LAI value produces the same TOC reflectance as illustrated in Fig. 8ac. For example a LAI of 4 m^2 m^{-2} at CC=95% resulted in a similar BRF compared to a LAI value of about 10 m^2 m^{-2}. The same phenomenon was observed also for the other bands of green (559 nm), red edge (727 nm), and near-infrared wavelengths (736, 745, 755, and 764 nm), except the red (671 nm) band, which is strongly driven by the chlorophyll absorption. However, the introduction of mixed cells decreased the overall nadir NIR BRF and reduced the intensity of this phenomenon by compensating an increase of BRF values for low LAI (Fig. 8e). This is most probably due to higher NIR refraction of twig bark being propagated through sparse canopies. Fig. 8bdf show a stronger monotypic negative correlation between LAI and NIR BRF of the shaded crown pixels for all CC categories. Shaded canopy signatures were less affected by the mixed cells, because the results of scenario F and FW appeared to be almost similar and only a minor shift of BRF (about 1–2%) was observed for scenario FWT. Similarly, the signal of the overall canopy reflectance remained monotonic, with descending BRF for increasing LAI values.

3.2. Validation of the DART scenarios against the AISA BRF measurements

The cross-comparison of the atmospherically corrected AISA BRF and ground measured nadir reflectance of three selected natural targets was used to validate the reliability of the AISA image processing procedures (Fig. 9). The reflectance of the calibration targets was measured using an ASD FieldSpec Pro spectroradiometer at nadir view. Given the centre positioning of the calibration targets and the nadir ground measurements, we approximate for this comparison HDRF ≈ BRF. The high spatial resolution of AISA and the size of the reflectance panels allow the selection of pure calibration pixels. In addition, both natural calibration surfaces, i.e. clay and gravel, showed a close match between the ground and AISA airborne measurements with a reflectance root mean square error (RMSE) of 0.23% for clay and 0.18% for gravel, computed for 39 spectral bands between 450 and 800 nm (Fig. 9abcd). A higher RMSE of 3.16% was obtained for the grass surface. A discrepancy of about 5% appeared between the

ground and airborne data for the grassland at NIR wavelengths (Fig. 9ef). Because the grass stand was quite uniform concerning the height and biodiversity, this discrepancy may be caused by the angular effects raised from structural differences (e.g. LAI and LAD) within the grass canopy measured by the ASD FieldSpec Pro spectroradiometer and the AISA scanner.

Fig. 10 shows the modelled DART scenarios in relation to the AISA BRF measurements extracted from the 12 sample matrices depicted in Fig. 6. The fractions of sunlit and shaded crown pixels of both sources were comparable due to the similar canopy closure of the DMI and AISA matrices. The smallest BRF differences were found for the shaded canopy pixels for all three scenarios (Fig. 10cfi). The computed RMSE between DART modelled and AISA measured BRF for the shaded canopy was nearly constant in green, red, and RE wavelengths, and it differed only in the NIR for scenario F (RMSE=2.26%) (Table 4). In spite of this, the variability of the shaded BRF was higher than variability of the sunlit BRF. Sunlit canopy reflectances demonstrated the best fit in three bands for scenario FWT. DART simulations for scenario F and FW systematically overestimated the BRF at 559, 727, and 783 nm (Fig. 10beh), while scenario FWT overestimated reflectances in the 671 nm band. The RMSE of sunlit BRF for scenario FWT was computed to be smaller than 1.24% including all four spectral bands. RMSE values of sunlit BRF up to 3.71% were obtained for scenario FW, and even up to 5.35% for scenario F. On the other hand, these scenarios demonstrated a BRF RMSE of only 0.09 and 0.10% for the 671 nm wavelength, while the RMSE

Table 4
Root mean square errors (RMSE) computed for BRF of four spectral bands of the experimental spruce canopy obtained from 12 matrices (10×10 m) placed over the AISA Eagle image and corresponding DART simulated BRF for all three considered scenarios

Spectral bands				
	559 [nm]	671 [nm]	727 [nm]	783 [nm]
RMSE of canopy BRF [%]				
Scenario F	0.35	0.21	2.67	3.50
Scenario FW	0.27	0.23	2.08	2.31
Scenario FWT	0.27	0.77	0.83	1.35
RMSE of sunlit BRF [%]				
Scenario F	1.05	0.09	4.57	5.35
Scenario FW	0.84	0.10	3.62	3.71
Scenario FWT	0.39	1.08	1.15	1.23
RMSE of shaded BRF [%]				
Scenario F	0.61	0.43	1.41	2.26
Scenario FW	0.60	0.42	1.24	1.79
Scenario FWT	0.55	0.48	1.17	1.89

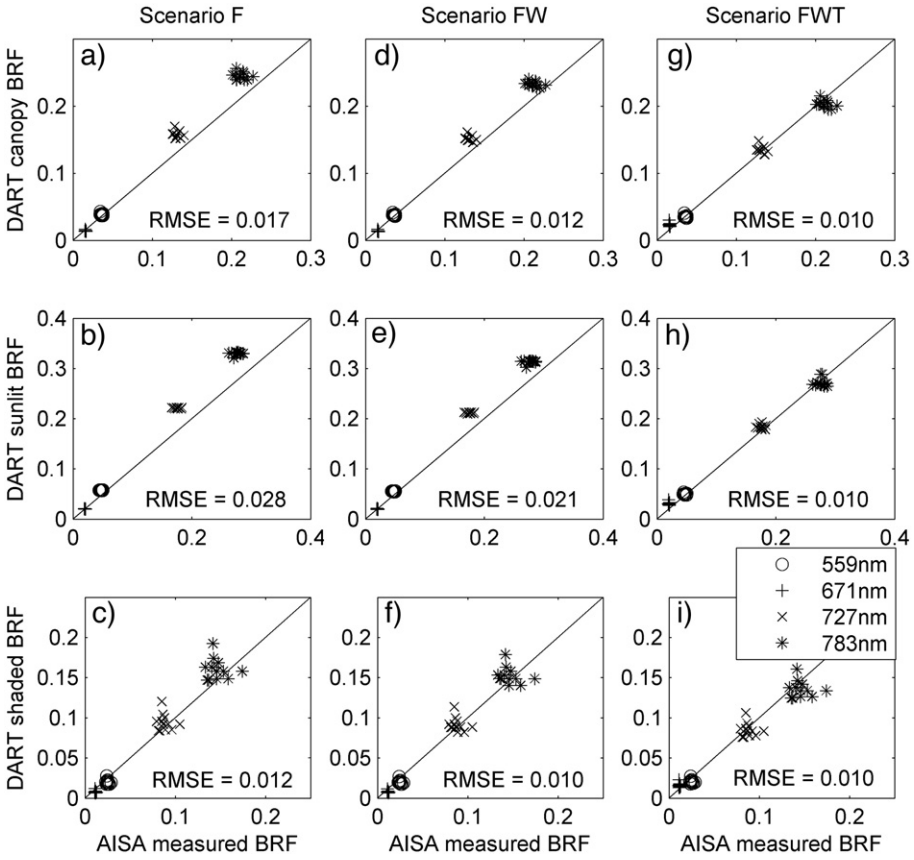

Fig. 10. Direct comparison of the AISA Eagle bidirectional reflectance factor (BRF) obtained from 12 sample areas (10×10 m) and corresponding DART simulated BRF for comparable fraction of sunlit and shaded crown parts, as well as whole spruce canopy for three scenarios: i) scenario F — only foliage (a, b, c), ii) scenario FW — leaves and major woody parts (d, e, f), and iii) scenario FWT — leaves, trunks, main branches, and small twigs (g, h, i) (RMSE=root mean square error).

was equal to 1.08% for the FWT scenario (Table 4). A similar pattern of BRF signatures and RMSE values was also obtained for the whole spruce canopy, mainly due to the contribution of the sunlit crown parts having a higher reflectance than the shaded parts (Fig. 10adg). In general, the best agreement between DART simulations and AISA Eagle measurements was obtained for the FWT scenario for all the tested spectral bands except the band at 671 nm wavelength.

3.3. Relation of vegetation indices with LAI at high spatial resolution

Two vegetation indices, NDVI and AVI, were computed for each DART modelled image. Design of the DMI allowed us to evaluate changes in the vegetation indices with increasing LAI for 10 subsequent canopy closures per scenario. Fig. 11 illustrates the relationship between the NDVI and LAI values. All the plots showed that the NDVI saturates for a LAI between 5 and 8 m^2 m^{-2}. Graphs for scenario F and FW have a very similar pattern, only the variability with the CC categories increased by introduction of the trunks and main branches and NDVI values are slightly lower (Fig. 11abcdef). A stronger decrease in NDVI values and even higher variability within the CC categories was noticed for scenario FWT (Fig. 11ghj). However, the NDVI values computed for the sunlit, shaded, and overall spruce canopy have a comparable range. It seems that this index is less sensitive to shadows within the canopy. Differences between the sunlit and shaded NDVI for the FWT scenario were almost negligible. In case of scenario F and FW, the sunlit NDVI was lower than the shaded NDVI, mainly for higher values of LAI, but still the absolute NDVI difference was quite small (about 0.10).

Sensitivities of the AVI index for canopy LAI are depicted in Fig. 12. The relationships are more complex than for the NDVI and they differ more between sunlit and shaded crown parts. The relationship for the sunlit AVI values appeared nearly flat, but for lower LAI values (3–7 m^2 m^{-2}) they show indications of a non-monotonic (Gaussian-like) behaviour. AVI values for the shaded crown parts exhibited an almost linear decrease within increasing LAI. The canopy AVI values were also gradually decreasing with increasing LAI, but they were levelled off by the strong influence of the sunlit pixels in case of low LAI (3–5 m^2 m^{-2}). Graphs for scenario F and FW showed a similar trend with lower AVI values for sunlit and consequently whole canopy simulations (Fig. 12abcdef). Resulting AVI values for the scenario FWT were systematically lowered by the mixed cells presence and their

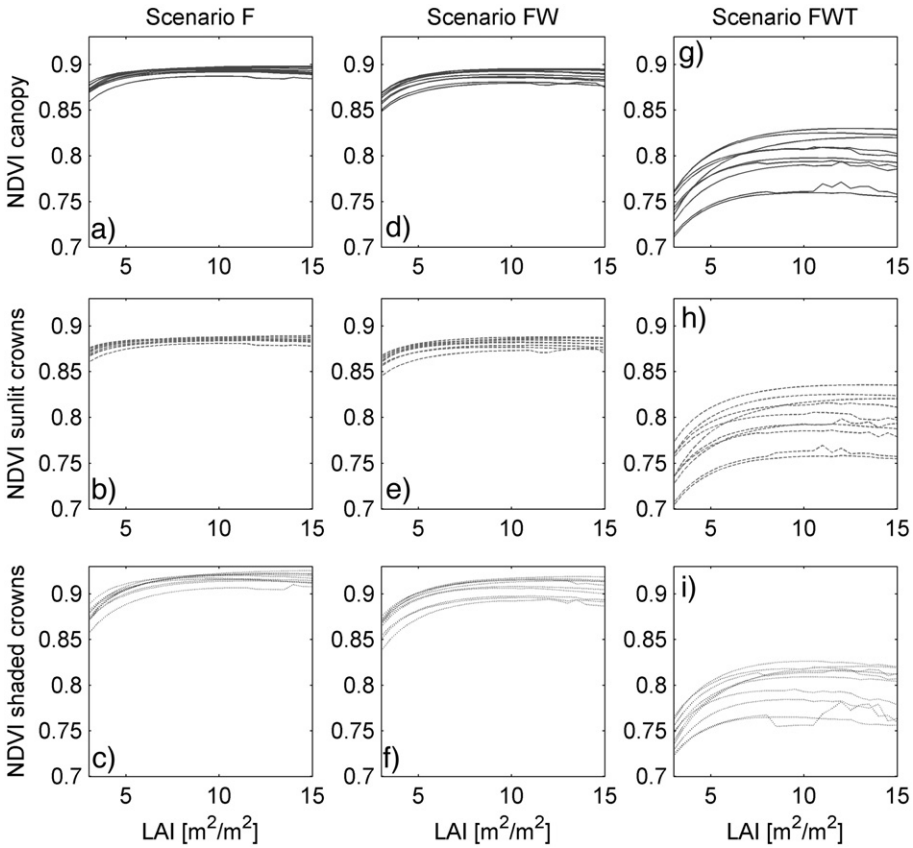

Fig. 11. Relationship between spruce canopy leaf area index (LAI) and normalized difference vegetation index (NDVI) displayed for sunlit, shaded, and total canopy reflectance simulated by the DART model within three scenarios: i) scenario F — only foliage (a, b, c), ii) scenario FW — leaves and major woody parts (d, e, f), and iii) scenario FWT — leaves, trunks, main branches, and small twigs (g, h, i). Each line represents one of ten simulated canopy closure categories (CC = 50, 55, 60, 65, 70, 75, 80, 85, 90, and 95%).

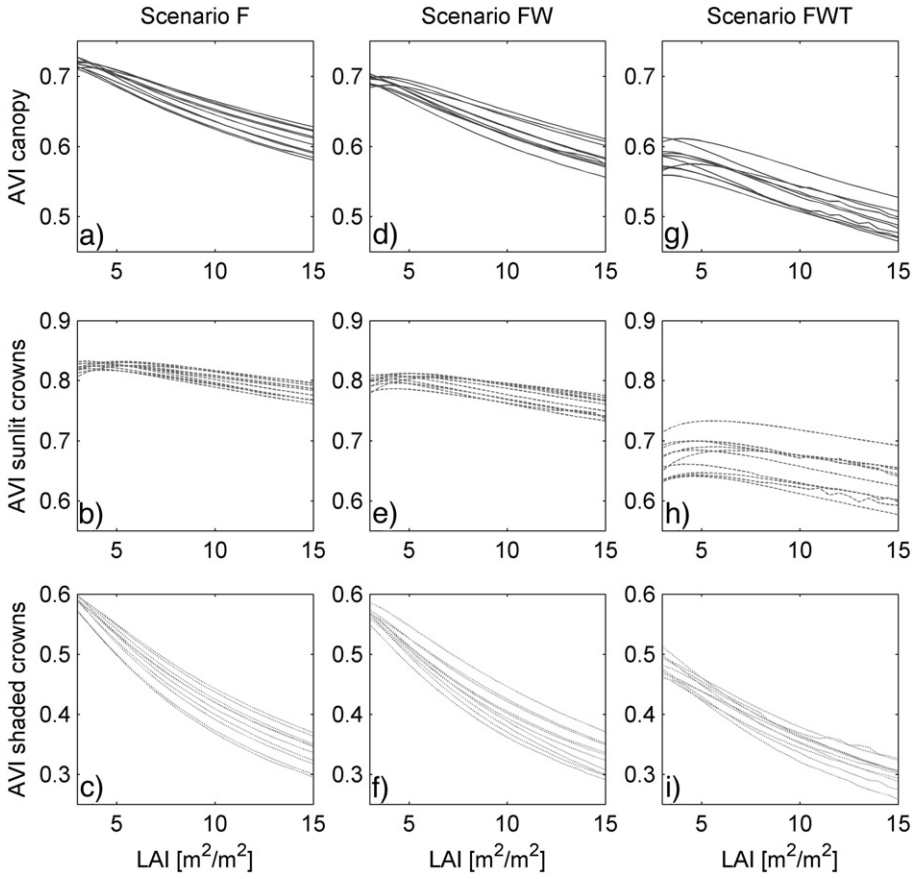

Fig. 12. Relationship between spruce canopy leaf area index (LAI) and angular vegetation index (AVI) plotted for sunlit, shaded, and total canopy reflectance simulated by the DART model within three scenarios: i) scenario F — only foliage (a, b, c), ii) scenario FW — leaves and major woody parts (d, e, f), and iii) scenario FWT — leaves, trunks, main branches, and small twigs (g, h, i). Each line represents one of ten simulated canopy closure categories (CC = 50, 55, 60, 65, 70, 75, 80, 85, 90, and 95%).

variability within the CC classes increased, especially for the sunlit crown parts (Fig. 12ghj).

4. Discussion

4.1. Influence of the woody elements on simulated reflectance

The results of our modelling experiment demonstrate that the woody elements, being still a minor contributor of a pixel's reflectance compared to the total amount of green foliage, influence noticeably the transfer of photons within the forest canopy. The DART modelled scenarios revealed that small woody twigs introduced into the leaf canopy play a more important role in forest RT than the robust woody parts like trunks and main branches. These robust woody parts caused only minor changes in the overall simulated canopy BRF (even for a forest stand with low LAI; c.f. Fig. 7), whereas the introduction of the mixed cells in DART clearly influenced the BRF at all investigated wavelengths. The total absence of photon transmittance and high photon absorbance by the woody elements decreased the NIR canopy reflectance, despite of the relatively high bark reflectance at NIR wavelengths. These findings are in agreement with results of Myneni et al. (1997). An opposite effect was observed at the red wavelength, where the mixed cells increased canopy reflectance by approximately 2%. This difference results from a high reflectance of the twig bark (about 25%; Fig. 4) that, combined with a strong absorption of the foliage pigments, increased the red canopy BRF. Nadir BRF of the shaded parts was less influenced by the introduction of the mixed cells of the turbid media and opaque surfaces than nadir BRF of the sunlit parts, most probably due to lower signal level in the shade. The latter were more sensitive especially at NIR wavelengths, the wavelengths mostly influenced by the canopy structural characteristics including the woody element properties.

Smolander and Stenberg (2003, 2005) introduced a within-shoot multiple scattering mechanism named the photon recollision probability (Panferov et al., 2001), which was lately nested by Disney et al. (2006) into a Monte Carlo ray tracing model of a pine coniferous canopy. It has been shown by Rautiainen and Stenberg (2005) that the multiple scattering shoot correction, included in a semi-physical forest reflectance model named PARAS, increased the accuracy of a simulated coniferous canopy radiometric response. The within-shoot scattering decreased slightly the red and significantly the NIR BRF of the modelled forest canopy. The approach using mixed cells, as tested in this study, is aiming at the improvement of multiple scattering simulations within the forest canopy in general. However, it is not modelling coniferous shoot and

within-shoot needle clumping in full geometrical detail. The mixed cells concept was not designed as a feature specific for the coniferous crowns, but as a universal parameter common for any woody forest canopy. Its physical and mathematical background is differing from the photon recollision probability (Knyazikhin et al., 2005) and will be discussed in scientific literature as well (Martin & Gastellu–Etchegorry, personal communication). Still, the results of both of these approaches are not contradictory, but are showing similar general trends of decreasing coniferous canopy reflectance mainly in NIR part of the electromagnetic spectrum.

4.2. Reliability of the DART simulations

The comparison of the DART modelled nadir BRF and the atmospherically corrected AISA Eagle BRF for 12 specific forest patches (Fig. 6) showed the best agreement for the scenario FWT. However, the results of the other two scenarios were also close to the AISA measurements (the highest BRF RMSE was about 5% in the NIR). It must also be assumed that some uncertainties in the airborne image due to atmospheric and radiometric corrections remain. However, they were minimized by a vicarious calibration approach using three calibration targets (clay, gravel, and grass surface), which demonstrate the high accuracy of the AISA image calibration and correction. The only discrepancy in the data was found to be in the NIR plateau of the grass spectral target, which has been explained by the angular differences in the measured grass canopy.

The DART simulations of the scenario FWT suffered from a BRF overestimation in the red spectral band, most probably due to inaccurate parameterisation of the twig optical properties. These were assumed to be similar to the bark of large branches and uniform within the whole crown. Epiphytic green algae and lichens, dispersed irregularly throughout the canopy, often populate the bark of the spruce branches and twigs. The microstructure of their thalli should not interfere the NIR optical properties of the woody element bark, but some of them contain chlorophyll pigments, which increase red absorption and lower red reflectance of the bark. Consequently, the spatially distributed effect of epiphytic green algae and lichens, included into the twig and branch optical properties, could possibly reduce the red reflectance overestimation.

4.3. Consequences on LAI retrieval and vegetation indices

The most important wavelength with respect to the retrieval of forest LAI, are at the NIR plateau between 730 and 900 nm (considering the spectral range being confined to λ=400–1000 nm). Wavelengths of λ=400–730 nm are strongly influenced by the specific absorption of plant pigments (chlorophyll, carotenoids, etc.), and wavelengths of λ>900 nm by the specific absorption of water (Gates et al., 1965; Fukshansky, 1991). Higher concentration of these plant leaf components rule the reflectance and transmittance at the mentioned wavelengths and thus these are less sensitive, and consequently less suitable, for inversion of the structural canopy properties, including LAI. The DART modelled images showed a minimum influence of simulated woody elements on the reflectance between 730 and 900 nm for shaded crown parts, but a regular reflectance decrease within these wavelengths for the sunlit canopy parts. The average decline of the overall spruce canopy NIR BRF of about 4% represents a strong argument to include the small woody elements into the radiative transfer model targeting the forest LAI inversion.

One can observe the increase of the BRF heterogeneity within the CC categories of the same LAI values after inclusion of the mixed cells into the DART simulations (c.f. Fig. 7). This effect can potentially disturb the overall accuracy of the LAI retrieved for a forest canopy. Therefore, any LAI retrieving algorithm specifically designed for high spatial resolution image data should take into account the canopy closure as being a sensitive parameter driving the inversion quality.

With respect to the vegetation indices, the NDVI was found to be sensitive to tiny twig appearance within the simulated canopy. This can be explained by the fact that presence of the mixed cells caused a negatively correlated shift between the NIR and red canopy reflectance. Consequently, the ratios of the differences and sums of these bands decreased the NDVI values. However, minor irregularities were observed for the lower CC of the FWT scenario (Fig. 11ghj). These irregularities appeared due to the higher heterogeneity of canopy BRF after small twig introduction. Additionally, the results of all the DART simulations showed that NDVI is not a suitable tool for LAI inversion at very high spatial resolution, due to the fast saturation of the LAI-NDVI relationship. Nevertheless, Fig. 11 implies that this relationship for the FWT scenario saturates at higher LAI values than for the other scenarios.

The AVI values decreased with increasing LAI for simulations of the third FWT scenario. This originates from a reflectance decrease in the green and NIR and an increase in the red part. Such a spectral behaviour caused a widening of the angle between the lines connecting green with red and red with NIR reflectance and consequently a drop of the index value. The relation between canopy LAI and AVI disclosed a linearly decreasing function, but only for LAI values larger than 5.0 m^2 m^{-2}. This fact makes AVI not to be fully suitable for the canopy LAI retrieval either. However, no quantification of the effect on LAI retrieval was carried out, because the index computation is based on two wavelengths strongly influenced by the chlorophyll concentration, which was used in the DART modelling as a fixed parameter.

5. Conclusions

In this study we have investigated the influence of woody elements, i.e. trunks additionally composed of main branches and tiny twigs, on the TOC reflectance of a Norway spruce canopy at very high spatial resolution. The inclusion of trunks including first order branches into the DART model had a minor impact on the nadir reflectance of the simulated canopy. However, the introduction of mixed cells (Table 1) noticeably reduced nadir TOC reflectance at NIR wavelengths. This TOC BRF reduction can mainly be observed in the sunlit part of the simulated canopy, whereas the reflectance of the shaded canopy part remained almost unchanged. These findings were

confirmed by the direct comparison of the DART modelled images with atmospherically corrected airborne hyperspectral data. The study findings particularly highlighted the importance of sensitivity analyses dealing with the radiative transfer through complex forest canopies. The introduction of additional input parameters results in an increase of the RT model complexity, but also in a decrease of its invertability (Combal et al., 2003). Nevertheless, if sound a priori knowledge on the model input parameters is used, it may reduce the ill-posed inverse problem and increase the accuracy of the retrieved parameters.

More specifically, the inclusion and distribution of wood abundance in RT based approaches targeting at LAI retrieval at very high spatial resolution is a prerequisite when analyzing individual tree crowns. In particular the spatial distribution of small twig elements within the leaf canopy, being an important photon absorbing and scattering mechanism, significantly improves the retrieval. Also the findings on using two vegetation indices (NDVI, AVI) favour the physical LAI retrieval based inversion of the RT model rather than using empirical inversion based on establishing a statistical relationship between LAI and these indices.

Significant relevance will be attributed in the future to (3D) radiative transfer based inversion approaches for the retrieval of biophysical and biochemical variables. Where current approaches already rely on biome or ecosystem specific parameterization of the RT, future approaches will increasingly rely on more detailed parameterization of vegetation specific properties, such as plant functional types, species composition and the like. The inclusion of woody trunks, main branches and tiny twigs in DART demonstrated in a Norway spruce canopy in this paper confirm this trend.

Acknowledgements

This study was carried out within the ESA/PECS project No. 98029 and the Research Plan AV0Z6087904 of the Institute of System Biology and Ecology, Academy of Sciences of the Czech Republic. Zbyněk Malenovský likes to acknowledge the financial support from the Sabbatical Fellowship 1K04 provided by the Ministry of Education, Youth and Sports of the Czech Republic.

References

Ahl, D. E., Gower, S. T., Mackay, D. S., Burrows, S. N., Norman, J. M., & Diak, G. R. (2004). Heterogeneity of light use efficiency in a northern Wisconsin forest: Implications for modeling net primary production with remote sensing. *Remote Sensing of Environment*, *93*, 168−178.

Arora, V. K. (2002). Modeling vegetation as a dynamic component in soil–vegetation–atmosphere transfer schemes and hydrological models. *Reviews of Geophysics*, *40*, 1−3.

Atzberger, C. (2004). Object-based retrieval of biophysical canopy variables using artificial neural nets and radiative transfer models. *Remote Sensing of Environment*, *93*, 53−67.

Bannari, A., Morin, D., Bonn, F., & Huete, A. R. (1995). A review of vegetation indices. *Remote Sensing Reviews*, *13*, 95−120.

Broge, N. H., & Leblanc, E. (2001). Comparing prediction power and stability of broadband and hyperspectral vegetation indices for estimation of green leaf area index and canopy chlorophyll density. *Remote Sensing of Environment*, *76*, 156−172.

Campbell, G. S. (1990). Derivation of an angle density function for canopies with ellipsoidal leaf angle distributions. *Agricultural and Forest Meteorology*, *49*, 173−176.

Centre d'Etudes Spatiales de la Biosphère (CESBIO) (2005). *DART (Discrete Anisotropic Radiative Transfer)*. France: CESBIO Web page available online on http://www.cesbio.ups-tlse.fr/us/dart0.htm, Accessed November 30, 2005.

Chen, J. M., & Black, T. A. (1991). Measuring leaf area index of plant canopies with branch architecture. *Agricultural and Forest Meteorology*, *57*, 1−12.

Chen, J. M., & Black, T. A. (1992). Defining leaf area index for non-flat leaves. *Plant, Cell and Environment*, *15*, 421−429.

Chen, J. M., & Leblanc, S. G. (1997). A four-scale bidirectional reflectance model based on canopy architecture. *Ieee Transactions on Geoscience and Remote Sensing*, *35*, 1316−1337.

Clevers, J. G. P. W. (1988). Multispectral aerial-photography as a new method in agricultural field trial analysis. *International Journal of Remote Sensing*, *9*, 319−332.

Combal, B., Baret, F., Weiss, M., Trubuil, A., Mace, D., Pragnere, A., et al. (2003). Retrieval of canopy biophysical variables from bidirectional reflectance: Using prior information to solve the ill-posed inverse problem. *Remote Sensing of Environment*, *84*, 1−15.

Cudlín, P., Novotný, R., Moravec, I., & Chmeliková, E. (2001). Retrospective evaluation of the response of montane forest ecosystems to multiple stress. *Ekologia (Bratislava)*, *20*, 108−124.

Daughtry, C. S. T., Biehl, L. L., & Ranson, K. J. (1989). A new technique to measure the spectral properties of conifer needles. *Remote Sensing of Environment*, *27*, 81−91.

Disney, M., Lewis, P., & Saich, P. (2006). 3D modelling of forest canopy structure for remote sensing simulations in the optical and microwave domains. *Remote Sensing of Environment*, *100*, 114−132.

Dzierzon, H., Sievanen, R., Kurth, W., Perttunen, J., & Sloboda, B. (2003). Enhanced possibilities for analyzing tree structure as provided by an interface between different modelling systems. *Silva Fennica*, *37*, 31−44.

Fang, H., & Liang, S. (2005). A hybrid inversion method for mapping leaf area index from MODIS data: Experiments and application to broadleaf and needleleaf canopies. *Remote Sensing of Environment*, *94*, 405−424.

Fassnacht, K. S., Gower, S. T., MacKenzie, M. D., Nordheim, E. V., & Lillesand, T. M. (1997). Estimating the leaf area index of North Central Wisconsin forests using the landsat thematic mapper. *Remote Sensing of Environment*, *61*, 229−245.

Fukshansky, L. (1991). Photon transport in leaf tissue: Applications in plant physiology. In R. B. Myneni & J. Ross (Eds.), *Photon–vegetation interactions: applications in optical remote sensing and plant ecology* (pp. 253−302). Berlin: Springer–Verlag.

Gascon, F., Gastellu-Etchegorry, J. P., & Lefevre, M. J. (2001). Radiative transfer model for simulating high-resolution satellite images. *Ieee Transactions on Geoscience and Remote Sensing*, *39*, 1922−1926.

Gascon, F., Gastellu-Etchegorry, J. P., Lefevre-Fonollosa, M. J., & Dufrene, E. (2004). Retrieval of forest biophysical variables by inverting a 3-D radiative transfer model and using high and very high resolution imagery. *International Journal of Remote Sensing*, *25*, 5601−5616.

Gastellu-Etchegorry, J. P., Demarez, V., Pinel, V., & Zagolski, F. (1996). Modeling radiative transfer in heterogeneous 3-D vegetation canopies. *Remote Sensing of Environment*, *58*, 131−156.

Gastellu-Etchegorry, J. P., Martin, E., & Gascon, F. (2004). DART: a 3D model for simulating satellite images and studying surface radiation budget. *International Journal of Remote Sensing*, *25*, 73−96.

Gates, D. M., Keegan, J. C., & Prentice, K. C. (1965). Spectral properties of plants. *Applied Optics*, *4*, 11−20.

Gower, S. T. (2003). Patterns and mechanisms of the forest carbon cycle. *Annual Review of Environment and Resources*, *28*, 169−204.

Gower, S. T., Krankina, O., Olson, R. J., Apps, M., Linder, S., & Wang, C. (2001). Net primary production and carbon allocation patterns of boreal forest ecosystems. *Ecological Applications*, *11*, 1395−1411.

Gruber, F. (1994). Morphology of coniferous trees: possible effects of soil acidification on the morphology of Norway spruce and Silver fir. In D. L.

Godbold & A. Hüttermann (Eds.), *Effects of acid rain on forest processes* (pp. 265−324). New York: Wiley-Liss.

Haboudane, D., Miller, J. R., Tremblay, N., Zarco-Tejada, P. J., & Dextraze, L. (2002). Integrated narrow-band vegetation indices for prediction of crop chlorophyll content for application to precision agriculture. *Remote Sensing of Environment*, *81*, 416−426.

Hoffmann, W. A., & Jackson, R. B. (2000). Vegetation–climate feedbacks in the conversion of tropical savanna to Grassland. *Journal of Climate*, *13*, 1593−1602.

Ishii, H., Ford, E. D., Boscolo, M. E., Manriquez, A. C., Wilson, M. E., & Hinckley, T. M. (2002). Variation in specific needle area of old-growth Douglas-fir in relation to needle age, within-crown position and epicormic shoot production. *Tree Physiology*, *22*, 31−40.

Ishii, H., & McDowell, N. (2002). Age-related development of crown structure in coastal Douglas-fir trees. *Forest Ecology and Management*, *169*, 257−270.

Jonckheere, I., Fleck, S., Nackaerts, K., Muys, B., Coppin, P., Weiss, M., et al. (2004). Review of methods for in situ leaf area index determination Part I. Theories, sensors and hemispherical photography. *Agricultural and Forest Meteorology*, *121*, 19−35.

Jordan, C. F. (1969). Deviation of leaf-area index from quality of light on the forest floor. *Ecology*, *50*, 663−666.

Knyazikhin, Y., Marshak, A., & Myneni, R. (2005). Three-dimensional radiative transfer in vegetation canopies. In A. Davis & A. Marshak (Eds.), *Three-dimensional radiative transfer in the cloudy atmosphere* (pp. 617−651). New York: Springer−Verlag.

Knyazikhin, Y., Martonchik, J. V., Diner, D. J., Myneni, R. B., Verstraete, M., Pinty, B., et al. (1998). Estimation of vegetation canopy leaf area index and fraction of absorbed photosynthetically active radiation from atmosphere-corrected MISR data. *Journal of Geophysical Research-Atmospheres*, *103*, 32239−32256.

Koetz, B., Baret, F., Poilvé, H., & Hill, J. (2005). Use of coupled canopy structure dynamic and radiative transfer models to estimate biophysical canopy characteristics. *Remote Sensing of Environment*, *95*, 115−124.

Kratochvilová, I., Janouš, D., Marek, M. V., Barták, M., & Říha, L. (1989). Production activity of mountain cultivated Norway spruce stands under the impact of air pollution. *Ekologia (Bratislava)*, *8*, 407−419.

Kucharik, C. J., Foley, J. A., Delire, C., Fisher, V. A., Coe, M. T., Lenters, J. D., et al. (2000). Testing the performance of a Dynamic Global Ecosystem Model: Water balance, carbon balance, and vegetation structure. *Global Biogeochemical Cycles*, *14*, 795−825.

Kucharik, C. J., Norman, J. M., & Gower, S. T. (1998). Measurements of branch area and adjusting leaf area index indirect measurements. *Agricultural and Forest Meteorology*, *91*, 69−88.

Kuuluvainen, T., & Sprugel, D. G. (1996). Examining age- and altitude-related variation in tree architecture and needle efficiency in Norway spruce using trend surface analysis. *Forest Ecology and Management*, *88*, 237−247.

Leblanc, S. G., Bicheron, P., Chen, J. M., Leroy, M., & Cihlar, J. (1999). Investigation of directional reflectance in boreal forests with an improved four-scale model and airborne POLDER data. *Ieee Transactions on Geoscience and Remote Sensing*, *37*, 1396−1414.

Lee, K. -S., Cohen, W. B., Kennedy, R. E., Maiersperger, T. K., & Gower, S. T. (2004). Hyperspectral versus multispectral data for estimating leaf area index in four different biomes. *Remote Sensing of Environment*, *91*, 508−520.

Li-Cor (1983). *1800–12 integrating sphere instruction manual. Publication number 8305–0034.* pp.

Malenovský, Z., Martin, E., Gastellu_Etchegorry, J. P., Cudlín, P., & Clevers, J. G. P. W. (2003). Heterogeneity description improvements of spruce crown architecture simulated using the 3D radiative transfer model DART. *Proceedings of the 2nd SPECTRA Workshop*, 28._ 30. October 2003, ESTEC, Noordwijk, The Netherlands: European Space Agency.

Martonchik, J. V., Bruegge, C. J., & Strahler, A. H. (2000). A review of reflectance nomenclature used in remote sensing. *Remote Sensing Reviews*, *19*, 9−20.

Mesarch, M. A., Walter-Shea, E. A., Asner, G. P., Middleton, E. M., & Chan, S. S. (1999). A revised measurement methodology for conifer needles spectral optical properties: Evaluating the influence of gaps between elements. *Remote Sensing of Environment*, *68*, 177−192.

Middleton, E. M., Walter-Shea, E. A., Mesarch, M. A., Chan, S. S., & Rusin, R. J. (1997). Optical properties of Black spruce and Jack pine needles at BOREAS sites in Saskatchewan, Canada. *Canadian Journal of Remote Sensing*, *23*, 109−119.

Monteith, J. L., & Unsworth, M. H. (1990). *Principles of Environmental Physics* (pp. 291) (2nd edn). London: Edward Arnold.

Myneni, R. B., Hoffman, S., Knyazikhin, Y., Privette, J. L., Glassy, J., Tian, Y., et al. (2002). Global products of vegetation leaf area and fraction absorbed PAR from year one of MODIS data. *Remote Sensing of Environment*, *83*, 214−231.

Myneni, R. B., Nemani, R. R., & Running, S. W. (1997). Estimation of global leaf area index and absorbed par using radiative transfer models. *Ieee Transactions on Geoscience and Remote Sensing*, *35*, 1380−1393.

Nicolini, E., Chanson, B., & Bonne, F. (2001). Stem growth and epicormic branch formation in understorey beech trees (*Fagus sylvatica* L.). *Annals of Botany*, *87*, 737−750.

North, P. R. J. (2002). Estimation of fAPAR, LAI, and vegetation fractional cover from ATSR-2 imagery. *Remote Sensing of Environment*, *80*, 114−121.

Oak Ridge National Laboratory Distributed Active Archive Center (ORNL DAAC) (2005). FLUXNET A Global Network Integrating Worldwide CO_2 Flux Measurements. Web page available on-line on. http://www.fluxnet.ornl.gov/fluxnet/index.cfm Oak Ridge, Tennessee, USA, Accessed November 30, 2005.

Oak Ridge National Laboratory Distributed Active Archive Center (ORNL DAAC) (2005). MODIS ASCII Subsets. Web page available on-line on. http://www.modis.ornl.gov/modis/index.cfm Oak Ridge, Tennessee, USA, Accessed November 30, 2005.

Panferov, O., Knyazikhin, Y., Myneni, R. B., Szarzynski, J., Engwald, S., Schnitzler, K. G., et al. (2001). The role of canopy structure in the spectral variation of transmission and absorption of solar radiation in vegetation canopies. *Ieee Transactions on Geoscience and Remote Sensing*, *39*, 241−253.

Pavelka, M., Janouš, D., Urban, O., Acosta, M., Pokorný, R., Havránková, K., et al. (2003). Carbon sources in vertical profile of a Norway spruce stand. *Folia Oecologica*, *30*, 199−206.

Pinty, B., Widlowski, J. L., Taberner, M., Gobron, N., Verstraete, M. M., Disney, M., et al. (2004). Radiation Transfer Model Intercomparison (RAMI) exercise: Results from the second phase. *Journal of Geophysical Research-Atmospheres*, 109.

Plummer, S. E., North, P. R., & Briggs, S. A. (1994). The Angular Vegetation Index: an atmospherically resistant index for the second along track scanning radiometer (ATSR-2). *Proceedings of the 6th Symposium on Physical Measurements and Spectral Signatures in Remote Sensing, 17–21 January 1994* (pp. 717−722). Toulouse, France: CNES.

Pokorný, R., & Marek, M. V. (2000). Test of accuracy of LAI estimation by LAI-2000 under artificially changed leaf to wood area proportions. *Biologia Plantarum*, *43*, 537−544.

Rautiainen, M., & Stenberg, P. (2005). Application of photon recollision probability in coniferous canopy reflectance simulations. *Remote Sensing of Environment*, *96*, 98−107.

Remphrey, W. R., & Davidson, C. G. (1992). Spatiotemporal distribution of epicormic shoots and their architecture in branches of Fraxinus–Pennsylvanica. *Canadian Journal of Forest Research-Revue Canadienne De Recherche Forestiere*, *22*, 336−340.

Richter, R., & Schlapfer, D. (2002). Geo-atmospheric processing of airborne imaging spectrometry data. Part 2: atmospheric/topographic correction. *International Journal of Remote Sensing*, *23*, 2631−2649.

Rouse, J. W., Haas, R. H., Schell, J. A., & Deering, D. W. (1973). Monitoring vegetation systems in the great plains with ERTS. *Third ERTS Symposium, NASA SP-351*, *Vol. I*. (pp. 309−317).

Schaepman, M. E., Koetz, B., Schaepman-Strub, G., & Itten, K. I. (2005). Spectrodirectional remote sensing for the improved estimation of biophysical and-chemical variables: Two case studies. *International Journal of Applied Earth Observation and Geoinformation*, *6*, 271−282.

Schaepman-Strub, G., Schaepman, M., Dangel, S., Painter, T., & Martonchik, J. (2005). About the use of reflectance terminology in imaging spectroscopy. *EARSeL eProceedings*, *4*, 191−202.

Shabanov, N. V., Huang, D., Yang, W., Tan, B., Knyazikhin, Y., Myneni, R. B., et al. (2005). Analysis and optimization of the MODIS leaf area index

algorithm retrievals over broadleaf forests. *IEEE Transactions on Geoscience and Remote Sensing*, *43*, 1855−1865.

Shabanov, N. V., Wang, Y., Buermann, W., Dong, J., Hoffman, S., Smith, G. R., et al. (2003). Effect of foliage spatial heterogeneity in the MODIS LAI and FPAR algorithm over broadleaf forests. *Remote Sensing of Environment*, *85*, 410−423.

Smith, G. M., & Milton, E. J. (1999). The use of the empirical line method to calibrate remotely sensed data to reflectance. *International Journal of Remote Sensing*, *20*, 2653−2662.

Smolander, S., & Stenberg, P. (2003). A method to account for shoot scale clumping in coniferous canopy reflectance models. *Remote Sensing of Environment*, *88*, 363−373.

Smolander, S., & Stenberg, P. (2005). Simple parameterizations of the radiation budget of uniform broadleaved and coniferous canopies. *Remote Sensing of Environment*, *94*, 355−363.

Strahler, A. H. (1980). The use of prior probabilities in maximum-likelihood classification of remotely sensed data. *Remote Sensing of Environment*, *10*, 135−163.

Taylor, G. E. J. (1998). Forest ecosystems and air pollution: The importance of multiple stress interaction on a regional and global scale. In J. C. Cech, B. W. Wilson, & D. B. Crosby (Eds.), *Multiple stress in ecosystems* (pp. 23−40). Boca Raton: Lewis Publishers.

Tian, Y., Woodcock, C. E., Wang, Y., Privette, J. L., Shabanov, N. V., Zhou, L., et al. (2002). Multiscale analysis and validation of the MODIS LAI product I. Uncertainty assessment. *Remote Sensing of Environment*, *83*, 414−430.

Tian, Y., Woodcock, C. E., Wang, Y., Privette, J. L., Shabanov, N. V., Zhou, L., et al. (2002). Multiscale analysis and validation of the MODIS LAI product II. Sampling strategy. *Remote Sensing of Environment*, *83*, 431−441.

Tucker, C. J. (1979). Red and photographic infrared linear combinations for monitoring vegetation. *Remote Sensing of Environment*, *8*, 127−150.

Turner, D. P., Cohen, W. B., Kennedy, R. E., Fassnacht, K. S., & Briggs, J. M. (1999). Relationships between Leaf Area Index and Landsat TM spectral vegetation indices across three temperate zone sites. *Remote Sensing of Environment*, *70*, 52−68.

Turner, D. P., Ritts, W. D., Cohen, W. B., Gower, S. T., Zhao, M. S., Running, S. W., et al. (2003). Scaling Gross Primary Production (GPP) over boreal and deciduous forest landscapes in support of MODIS GPP product validation. *Remote Sensing of Environment*, *88*, 256−270.

Turner, D. P., Ritts, W. D., Cohen, W. B., Maeirsperger, T. K., Gower, S. T., Kirschbaum, A. A., et al. (2005). Site-level evaluation of satellite-based global terrestrial gross primary production and net primary production monitoring. *Global Change Biology*, *11*, 666−684.

Weiss, M. (2004). Review of methods for in situ leaf area index (LAI) determination Part II. Estimation of LAI, errors and sampling. *Agricultural and Forest Meteorology*, *121*, 37−53.

Zeng, N., & Neelin, J. D. (2000). The role of vegetation–climate interaction and interannual variability in shaping the African Savanna. *Journal of Climate*, *13*, 2665−2670.

Zhang, L., Dawes, W. R., & Walker, G. R. (2001). Response of mean annual evapotranspiration to vegetation changes at catchment scale. *Water Resources Research*, *37*, 701−708.